05 Feb 2013

A New Method for Online Flow Regime Monitoring in Bubble Column Reactors Via Nuclear Gauge Densitometry

Ashfaq Shaikh

Muthanna H. Al-Dahhan

Missouri University of Science and Technology, aldahhanm@mst.edu

Recommended Citation

A. Shaikh and M. H. Al-Dahhan, "A New Method for Online Flow Regime Monitoring in Bubble Column Reactors Via Nuclear Gauge Densitometry," *Chemical Engineering Science*, vol. 89, pp. 120 - 132, Elsevier, Feb 2013.

The definitive version is available at https://doi.org/10.1016/j.ces.2012.11.023

Chemical Engineering Science 89 (2013) 120–132

Contents lists available at SciVerse ScienceDirect

Chemical Engineering Science

journal homepage: www.elsevier.com/locate/ces

A new method for online flow regime monitoring in bubble column reactors via nuclear gauge densitometry

Ashfaq Shaikh [a,*], Muthanna Al-Dahhan [b]

[a] Eastman Research Division, Eastman Chemical Company, Kingsport, TN 37662, USA
[b] Missouri University of Science and Technology, Rolla, MO 65409, USA

HIGHLIGHTS

- We study nuclear gauge densitometry for flow regime demarcation in bubble column.
- This work proposes three easy-to-use flow regime identifiers for NGD.
- Flow regime footprints are identified without changing process conditions.

ARTICLE INFO

Article history:
Received 3 August 2012
Received in revised form
9 November 2012
Accepted 18 November 2012
Available online 28 November 2012

Keywords:
Bubble column
Flow regime
Nuclear gauge densitometry
Gas holdup
Regime transition
Hydrodynamics

ABSTRACT

In the current work, Nuclear gauge densitometry (NGD), which is commercially available and industrially used for liquid/slurry level measurement and control, has been employed to identify fingerprints of the prevailing hydrodynamic flow regime. Experiments were performed using an air–water system in 0.1012 m diameter and 1.2 m long bubble column at ambient pressure. The superficial gas velocities were varied from 1 cm/s to 12 cm/s with an interval of 0.5 cm/s near transition region. The flow regime boundaries were defined using the conventional methods of flow regime demarcation such as the change in the slope of the overall gas holdup and the drift flux plot. The obtained photon counts history was subjected to various time-series analyses. Based on the comparison with the results of conventional methods, objective flow regime identifiers for NGD were proposed. The obtained flow regime identifiers can be helpful for online flow regime monitoring in laboratory as well as industrial bubble column reactors.

1. Introduction

Bubble columns are two-phase gas-liquid systems in which a gas is dispersed through a sparger and bubbles through a liquid in vertical cylindrical columns, with or without internals such as heat exchangers. The gas phase contains one or more reactants, while the liquid phase usually contains product and/or reactants (or sometimes is inert). Generally, the operating liquid superficial velocity (in the range of 0–2 cm/s) is an order of magnitude smaller than the superficial gas velocity (1–50 cm/s). The bubble columns offer numerous advantages: good heat and mass transfer characteristics, no moving parts, reduced wear and tear, higher catalyst durability, ease of operation, and low operating and maintenance costs. One of the main disadvantages of bubble column reactors is significant back-mixing, which can affect product conversion.

Bubble column reactors have been used in chemical, petrochemical, biochemical, and pharmaceutical industries for various processes (Carra and Morbidelli, 1987; Deckwer, 1992; Fan, 1989). Examples of such processes are the partial oxidation of ethylene to acetaldehyde, wet-air oxidation (Deckwer, 1992), liquid phase methanol synthesis (LPMeOH), Fischer-Tropsch (FT) synthesis (Wender, 1996), hydrogenation of maleic acid (MAC), hydro conversion of heavy oils and petroleum feedstocks, cultivation of bacteria, cultivation of mold fungi, production of single cell protein, animal cell culture (Lehman and Hammer, 1978), and treatment of sewage (Diesterwerg et al., 1978).

In bubble columns, four types of flow patterns have been observed, viz., homogeneous (bubbly), heterogeneous (churn-turbulent), slug, and annular flow (Fig. 1). However, bubbly and churn-turbulent flow regimes are most frequently encountered. Depending upon the operating conditions, these two regimes can be separated by a transition regime In these different flow regimes, the interaction of the dispersed gas phase with the continuous liquid phase varies considerably.

The homogeneous flow regime generally occurs at low to moderate superficial gas velocities. It is characterized by uniformly sized small bubbles traveling vertically with minor transverse and axial oscillations. There is practically no coalescence

* Corresponding author. Tel.: +1 423 229 8840.
E-mail address: ashaikh@eastman.com (A. Shaikh).

0009-2509/$ - see front matter © 2012 Elsevier Ltd. All rights reserved.
http://dx.doi.org/10.1016/j.ces.2012.11.023

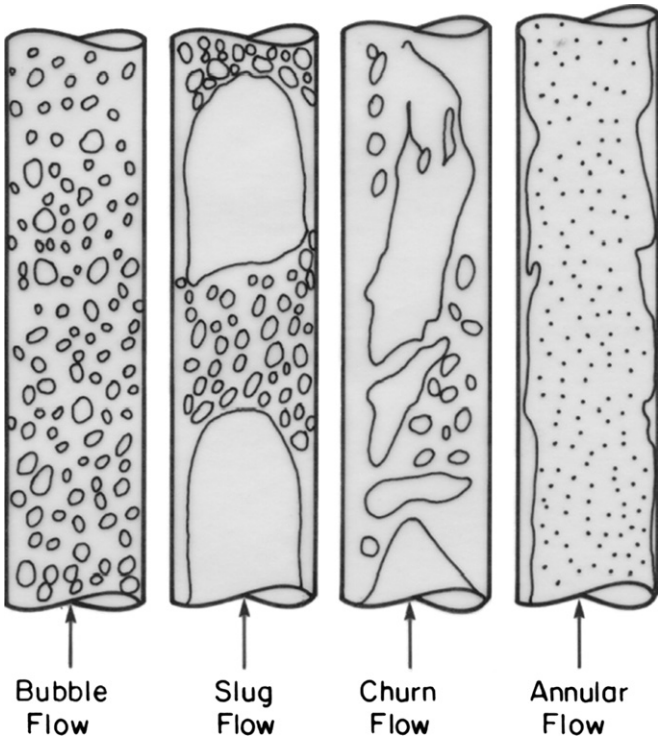

Fig. 1. Various flow regimes in bubble column reactors.

and break-up, hence there is a narrow bubble size distribution. The gas holdup distribution is radially uniform; therefore bulk liquid circulation is insignificant. The size of the bubbles depends mainly on the nature of the gas distribution and the physical properties of the liquid. While heterogeneous flow occurs at high gas superficial velocities. Due to intense coalescence and break-up, small as well large bubbles appear in this regime, leading to wide bubble size distribution. The large bubbles churn through the liquid, and thus, it is called as churn-turbulent flow. The non-uniform gas holdup distribution across the radial direction causes bulk liquid circulation in this flow regime.

As one can see, homogeneous and heterogeneous flow regimes have entirely different hydrodynamic characteristics. Such different hydrodynamic characteristics result in different mixing as well as heat and mass transfer rates in these flow regimes. Therefore, the demarcation of flow regimes becomes an important task in the design and scale up of such reactors.

Ample studies have been performed in the literature to demarcate flow regimes in bubble column reactors. These studies led to various experimental techniques and corresponding flow regime identifiers. The experimental methods used for regime transition identification can be broadly classified in the following groups (Shaikh and Al-Dahhan, 2007):

- Visual observation
- Evolution of global hydrodynamic parameter
- Temporal signatures of quantity related to hydrodynamics
- Advanced measurement techniques

1.1. Visual observation

Visual observation is the simplest method to study the flow pattern in bubble columns. The slow, vertically rising bubbles can be observed in the homogeneous regime. However, in the heterogeneous regime there is an intense interaction of bubbles, leading to gross circulation. It is difficult to pinpoint the exact transition velocity by visual observation. Moreover, this method can be useful only when the column is transparent.

1.2. Evolution of global hydrodynamic parameter

Because the global hydrodynamic parameters are manifestations of the prevailing flow patterns, they vary with the regimes. This fact has generally been utilized to identify flow regime transition point. Typically, the global hydrodynamics have been quantified based on overall gas holdup. The relationship between overall gas holdup and superficial gas velocity can be expressed as

$$\varepsilon_G \propto U_G^n \quad (1)$$

The overall gas holdup increases with an increase in superficial gas velocity. As can be seen in Fig. 2a (Shaikh and Al-Dahhan, 2005), the relationship between overall gas holdup and superficial gas velocity varies over a range of velocities. The relationship is almost linear ($n=0.8$–1) at low gas velocities, but with an intense non-linear interaction of bubbles at high gas velocities, the relationship between overall gas holdup and superficial gas velocity deviates from linearity. The value of n is less than 1 ($n=0.4$–0.6). Hence, the change in slope of the gas holdup curve can be identified as a regime transition point. Sometimes, gas holdup shows an S-shaped curve, depending upon operating and

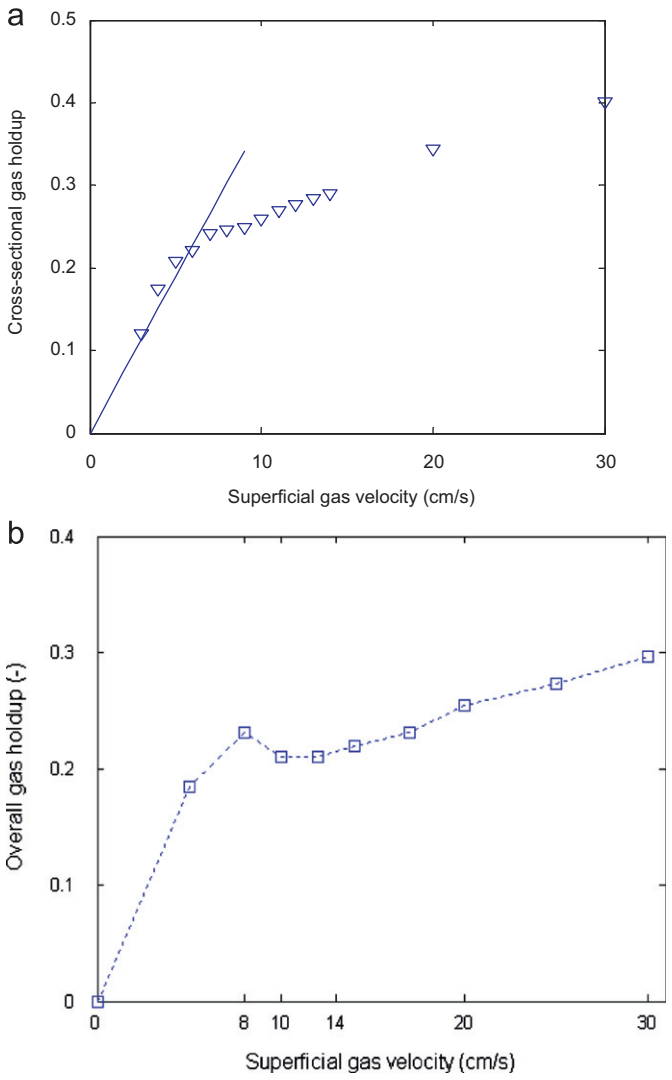

Fig. 2. Typical overall gas holdup curve (a) Shaikh and Al-Dahhan, 2005; and (b) Rados, 2003.

design conditions (Fig. 2b) [Rados, 2003]. In such cases, the superficial gas velocity at which maximum gas holdup has been attained is identified as the transition velocity.

However, when the change in slope is gradual or the gas holdup curve does not show a maximum in gas holdup, it is difficult to identify the transition point. In such cases, the drift flux method proposed by Wallis (1969) has been used extensively. In this method, the drift flux, j_{GL} (the volumetric flux of either phase relative to a surface moving at the volumetric average velocity) is plotted against the superficial gas velocity, U_G. The drift flux velocity is given by:

$$j_{GL} = U_G(1-\varepsilon_G) \pm U_L\varepsilon_G, \quad (2)$$

where ε_G is gas holdup and U_L is superficial liquid velocity. The positive or negative sign indicates counter-current or co-current flow of liquid relative to the gas phase, respectively.

1.3. Temporal signatures of quantity related to hydrodynamics

The global parameters represent macroscopic phenomena that are result of prevailing microscopic phenomena. Several attempts have been made to capture the instantaneous flow behavior through an energetic parameter.

The following temporal signatures have been utilized for flow regime transition:

- Pressure fluctuations [Nishikawa et al., 1969; Matsui, 1984; Drahos et al., 1991; Letzel et al., 1997; Vial et al., 2001, Park and Kim, 2003]
- Local holdup fluctuations using resistive or optical probes [Bakshi et al., 1995; Briens et al., 1997]
- Temperature fluctuations using a heat transfer probe [Thimmapuram et al., 1992]
- Local bubble frequency measured using an optical transmittance probe [Kikuchi et al., 1997]
- Conductivity probe [Zhang et al., 1997]
- Sound fluctuations using an acoustic probe [Holler et al., 2003; Al-Masry et al., 2005]

Various time-series analyses have been used to interpret the fluctuations of these parameters and to identify flow regimes and their transition. The commonly used time-series analyses are statistical analysis, autocorrelation analysis, stochastic modeling, spectral analysis, chaos analysis, and wavelet analysis. These time-series techniques are summarized elsewhere (Shaikh and Al-Dahhan, 2007).

1.4. Advanced measurement techniques

With advances in measurement techniques, various imaging and velocimetric techniques have been used in flow regime transition studies.

- Particle image velocimetry (PIV) [Chen et al., 1994; Lin et al., 1996]
- Electrical capacitance tomography (ECT) [Bennett et al., 1999]
- Electrical resistance tomography (ERT) [Dong et al., 2001; Murugaian et al., 2005]
- Laser Doppler anemometry (LDA) [Olmos et al., 2003]
- Computer automated radioactive particle tracking (CARPT) [Cassanello et al., 2001; Nedeltchev et al., 2003]
- Computed tomography [Shaikh and Al-Dahhan, 2005]

Although the implementation of advanced measurement techniques is relatively difficult, they provide detailed flow information and are useful in understanding prevailing phenomena.

The detailed review of various aspects of flow regimes in bubble columns by Shaikh and Al-Dahhan (2007) concluded that most flow regime studies appear to focus on determining transition velocity by observing the evolution of secondary parameters over a range of superficial gas velocities. However, there is a need to develop techniques and corresponding flow regime identifiers that can provide information regarding prevailing flow regimes in an existing process without changing the operating conditions. Such an approach can be used for online flow regime monitoring and troubleshooting in industry. However, it demands the use of a time-series analysis that is simple, robust, fast, and easily used by non-experts working in the plant.

Based on this, the objective of this work is to explore the potential of nuclear gauge densitometry (NGD) for demarcation of flow regimes and to propose the corresponding flow regime identifiers. The reason for exploring NGD lies in its robustness from an experimental point of view, both on the laboratory as well as the industrial scale. Of particular industrial interest is the fact that NGD can be implemented without disturbing the running operation. It is being currently used in industry for liquid/slurry level monitoring and control in chemical reactors as well as in various separators. Hence, NGD can be used either in chemically reacting or non-reacting system without any modifications.

2. Experimental setup

2.1. Nuclear gauge densitometry

Nuclear gauge densitometry (NGD) consists of a sealed source in a source holder and a scintillation detector in front of the source. The source holder is mounted on one side of a column, with the detector on the opposite side. A focused beam of radiation is transmitted from the source, through the column and process material, to the detector. As the density of the material in the column changes, the amount of radiation reaching the detector changes. It is generally believed that the amount of radiation that reaches the detector through the process material is reflective of its flow behavior and properties. Fig. 3 shows the schematics of NGD with a source and a detector in front of it.

NGD is used extensively in industry for such applications as level control, density measurement, interface identification, and weight measurements in conveyors. It is widely used in the following industries: chemicals, petrochemicals, off shore oil and gas, pharmaceuticals, cement, quarrying, solids handling, paper and

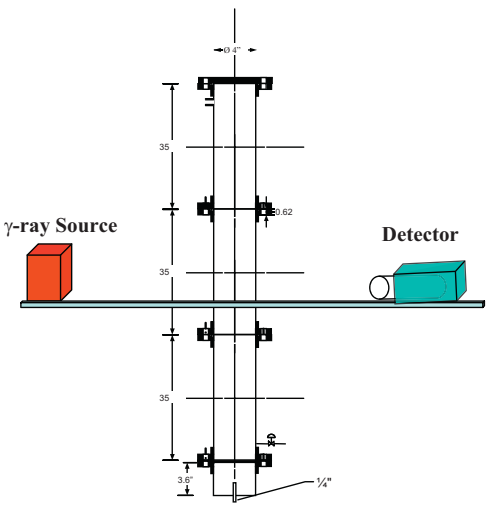

Fig. 3. Experimental setup for nuclear gauge densitometry (NGD).

food. The major advantages of NGD that make it attractive in everyday industrial use are (http://www.vegacontrols.com),

(i) Totally non-contact: Because the sources and detectors are mounted externally from the column or process, they are completely unaffected by the conditions inside, however extreme, providing reliable solutions when other technologies fail. They can be easily accessed, installed or removed without the process being affected or interrupted.
(ii) High integrity: A non-invasive system mounted outside the vessel means no exposure or wear by corrosive or abrasive products, and no need for construction to resist high pressure, high temperature process conditions. This means less risk of leaks or emissions, protecting processes, people and the environment.
(iii) High reliability and low maintenance: NGD measurements offer reliability and long term performance. In addition, source checking is routine, simple and can be planned well in advance.
(iv) Low installation costs: NGD can often be installed and commissioned without process shutdown. Also, on most applications, no alterations to the reactors/columns are needed, which means no expensive design changes for such implementation of NGD.

2.2. Experimental setup and conditions

The experimental setup consists of a laboratory scale plexiglass column (diameter=0.1012 m, height=1.2 m) as shown in Fig. 3. Air from the in-house utility line was fed through a sparger located at the bottom of the column. The gas flow rate was measured and adjusted by a rotameter (Dwyer Intruments Inc., model Rate Master). The sparger used in this study consists of 64 holes of 0.052″ diameter with an open area (% OA) of 1.09. The details of this experimental setup can be found elsewhere (Shaikh, 2007).

In this study, an existing CT setup was converted to NGD (Fig. 3) by placing a detector in front of an encapsulated γ-ray Cs-137 source ($\sim$100 mCi). The source and detector were mounted on a plate that can move in axial direction. The detector consists of a cylindrical 2×2 in. NaI crystal, a photo multiplicator (PM), and electronics, forming a 0.054×0.26 m cylindrical assembly. The collimator ($1/16''\times3/16''$) was placed in front of the detector. The photon count rate that was converted from the output voltage was collected through an automated data acquisition system. The superficial gas velocity was varied from 1 cm/s to 12 cm/s, with an interval of 0.5 cm/s, near the transition region. Air was used as the gas phase, while water ($\mu=1$ cP, $\rho=998$ kg m^{-3}, $\sigma=72$ dyne cm^{-1}) was the liquid phase.

Drahos et al. (1991) systematically examined the effect of various operating parameters on axial and radial profiles of the basic characteristics of pressure fluctuations. The signal measured in the bubble column is a complex function of the effects connected with formation, coalescence and passage of bubbles and their mutual interactions with the liquid phase eddies of various scales. Based on the cross-spectral studies, they showed that the characteristic frequencies are different, depending on the source (Table 1). Drahos et al. (1991) found that the interesting frequencies range from 0 Hz to 20 Hz for bubble columns. Hence, the photon counts history was obtained at an acquisition frequency of 50 Hz. In order to minimize statistical error in the various time-series analysis, a time-series with a total number of points, $N=15{,}000$, was collected (Smith, 1999). This requires a total acquisition time of 5 min. To check the consistency of the obtained data, the experiments were repeated three times.

Table 1
Characteristic frequencies in bubble column (Drahos et al., 1991).

Source	Order of characteristic frequencies (Hz)
Formation of bubbles	$>10^{1}$
Passage of bubbles	10^{0}–10^{1}
Coalescence of bubbles	10^{0}
Large-scale eddies	10^{-1}
Medium-size eddies	10^{0}
Liquid level fluctuations	10^{-2}–10^{-1}

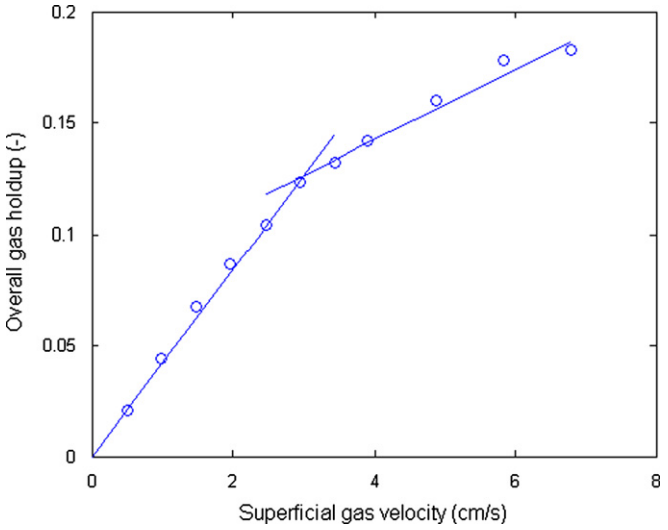

Fig. 4. Overall gas holdup curve using an air–water system at ambient conditions in a 0.1012 m diameter column.

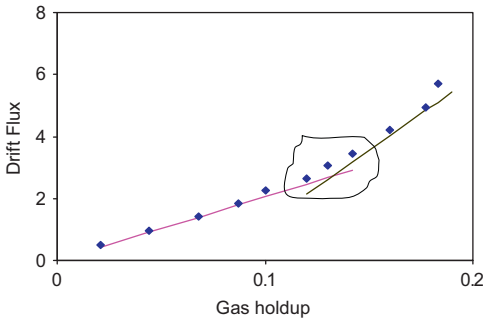

Fig. 5. Drift flux plot using an air-water system at ambient conditions in a 0.1012 m diameter column.

3. Results and discussion

3.1. Traditional analysis of flow regime transition

The flow regimes were first defined using traditional methods such as the change in the slope of the gas holdup curve and the change in the slope of the drift flux plot. The overall gas holdup was calculated by measuring the change in dynamic liquid height. Fig. 4 shows the evolution of overall gas holdup with superficial gas velocity. The overall gas holdup curve shows a change in slope around 3–4 cm/s, indicating flow regime transition.

Fig. 5 shows the drift flux plot in an air–water system at ambient conditions in a 0.1012 m diameter column. The drift flux curve also exhibits a change in the slope around 3–4 cm/s, confirming it to be the transition velocity.

Once the flow regime boundaries were defined using conventional methods, the obtained photon counts history was analyzed to

propose new "flow regime identifiers" for NGD. The characteristic behavior of photon counts history and also the derived information from the obtained time-series around the transition velocities, i.e., 3–4 cm/s will be utilized to propose such identifiers.

3.2. Analysis of photon counts history

Fig. 6 shows the photon counts history over 20 s of acquisition length for: (a) an empty column (air) and (b) water (without gas flow). The photon emission inherently shows Poisson distribution, where the mean and the variance of the obtained photon counts is the same. The photon counts history obtained in air and water (without gas flow) in the current study also shows Poisson distribution. In case of an empty column, the mean ≈ the variance = 265 while in water (no gas flow), the mean ≈ the variance = 130.

Fig. 7 shows the photon counts history received by the detector at various superficial gas velocities, (a) 1, (b) 3, (c) 7, and (d) 11 cm/s using air–water system at ambient conditions in a 0.1012 m diameter column. It clearly shows an increase in amplitude as well as oscillations in photon counts with an increase in superficial gas velocity. The photon counts fluctuations at low superficial gas velocities are relatively uniform, while at higher velocities, intense fluctuations can be observed, due to wide bubble size distribution. At higher velocities, large peaks can also be observed which are due to the presence of large bubbles in the path of γ-rays. The photon counts history appears to show the signature of the prevailing flow regime.

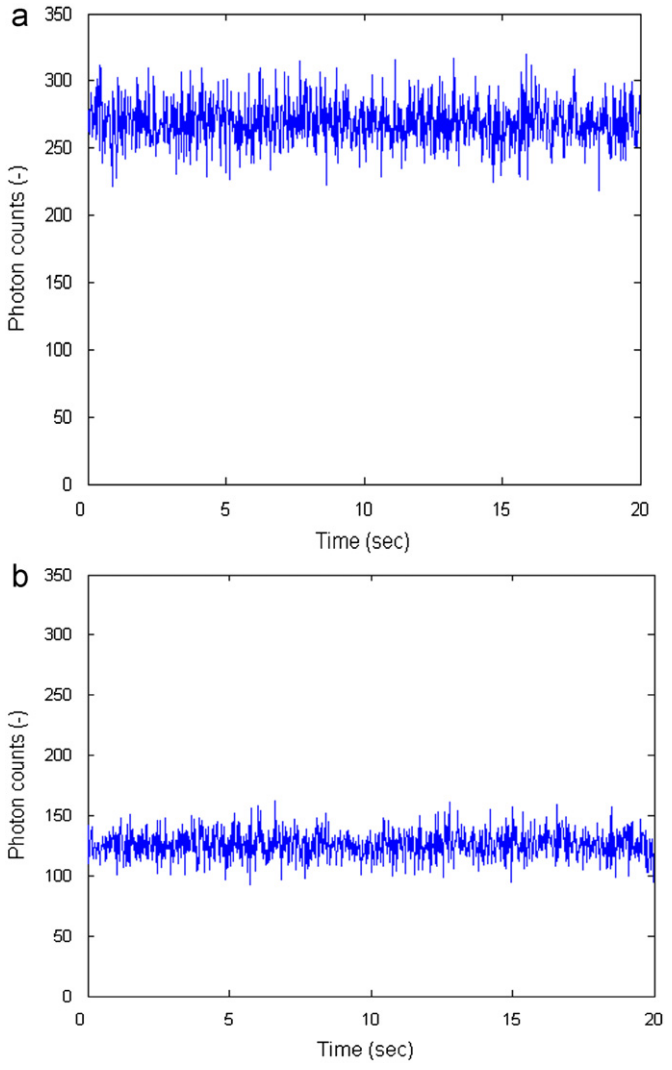

Fig. 6. Time-series of photon count fluctuations in a 0.1012 m diameter column in (a) empty column and (b) water (no gas flow).

The obtained photon counts history was subjected to various time-series analyses.

3.2.1. Statistical analysis

Statistical analysis is one of the obvious methods to study a time-series. The mean, μ is given by

$$\mu = \frac{\sum_{i=1}^{N} x_i}{N}. \tag{3}$$

The average deviation of a signal can be then written as

$$\text{Average deviation} = \frac{\sum_{i=1}^{N} |x_i - \mu|}{N}. \tag{4}$$

Although it is straightforward, the average deviation is almost never used in statistical analysis. The important parameter is not average deviation but the power represented by deviation from mean, called as the standard deviation, σ, or the variance, σ^2, and given as

$$\sigma^2 = \frac{\sum_{i=1}^{N} (x_i - \mu)^2}{(N-1)} \tag{5}$$

Fig. 8 shows the change in the second moment (i.e., the variance) of the photon counts history with superficial gas velocity. An increase in superficial gas velocity increases the variance of photon counts fluctuations. Around a superficial gas velocity of 3–4 cm/s, a noticeable increase in the variance with superficial gas velocity was observed. The variance versus superficial gas velocity relationship shows two distinct slopes. The change in the slope of the variance of the photons counts history was observed at 3–4 cm/s. Based on the conventional methods, the transition from homogeneous to heterogeneous flow also occurs at the same superficial gas velocities. Hence, a change in slope of the variance of photon counts history can be used to identify flow regime transition.

In the bubbly flow regime, the value of the slope of the variance is less, while in churn-turbulent flow a rapid increase in the variance with superficial gas velocity was observed. Apart from a Poisson distribution, the fluctuations in photon counts history are imparted by the passage of bubbles in the system. The value of the variance is low in bubbly flow, as small non-interacting bubbles with uniform sizes are present that result into lower photon counts fluctuations and the variance. However in churn-turbulent flow, both small and large bubbles are present, resulting in a wide bubble size distribution. In addition, there is an intense bubble–bubble interaction in this regime. In churn-turbulent flow, the γ-rays are frequently intercepted by bubbles of different sizes and intensity giving rise to higher fluctuations that result in higher value of the variance of the photon counts history. The two distinct slopes in the variance are mainly due to the different nature of bubble interactions and bubble size distribution in the two flow regimes. Hence, the change in the variance indicates the flow regime transition point.

3.2.2. Deviation from Poisson distribution

γ-rays inherently show Poisson distribution (i.e., the mean = the variance) in empty column as well as in water (no gas flow). Due to the introduction of gas in static water, the photon counts history deviates from a Poisson distribution because the photon counts obtained in a dynamic system have additional information characterizing the flow behavior. Hence, the deviation from Poisson distribution might be able to decipher information regarding the flow behavior and subsequently about the underlying flow regime. It was observed that with an increase in superficial gas velocity, the

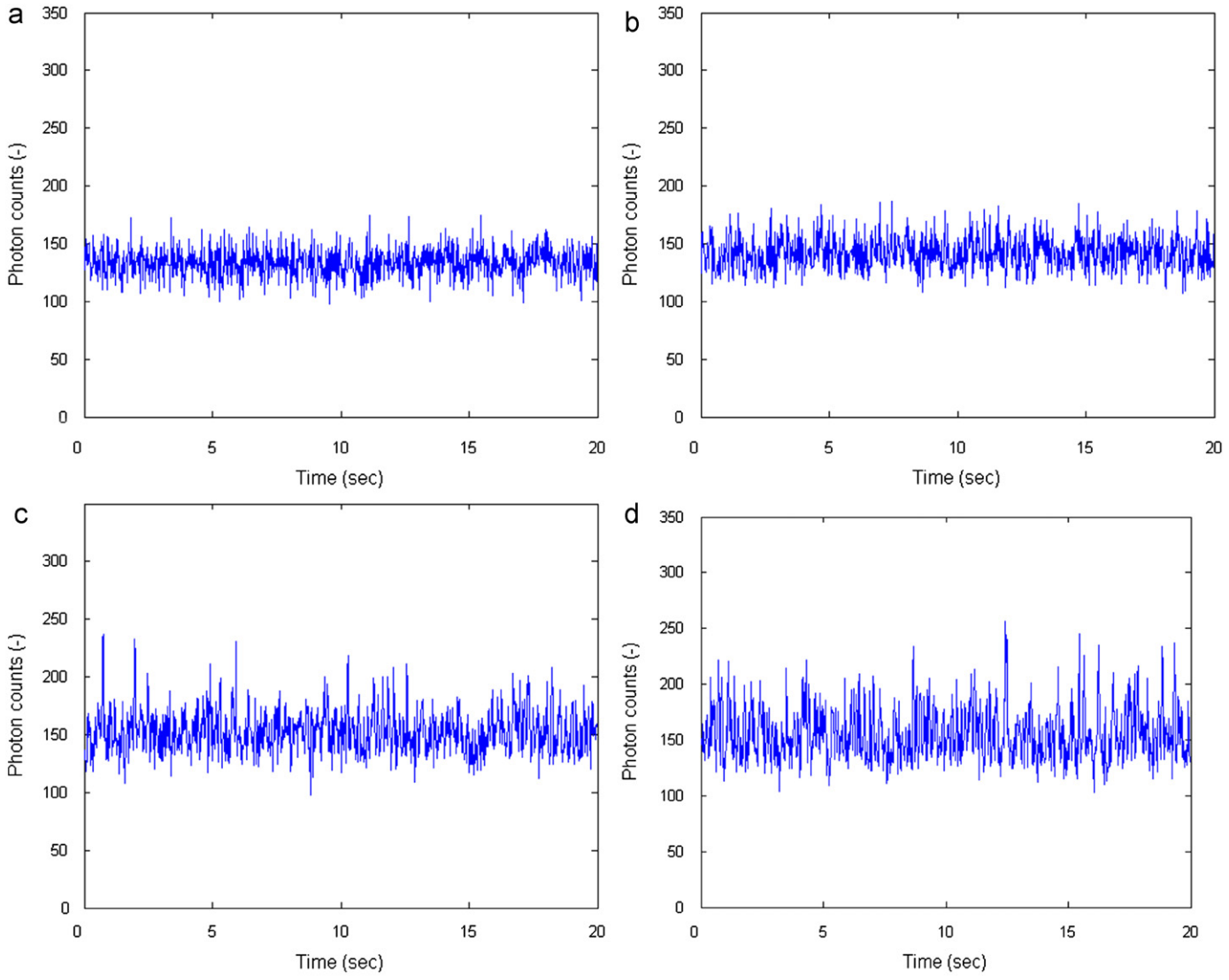

Fig. 7. Time-series of photon count fluctuations in a 0.1012 m diameter column using air-water system at superficial gas velocities of (a) 1, (b) 3, (c) 7, and (d) 11 cm/s at ambient conditions.

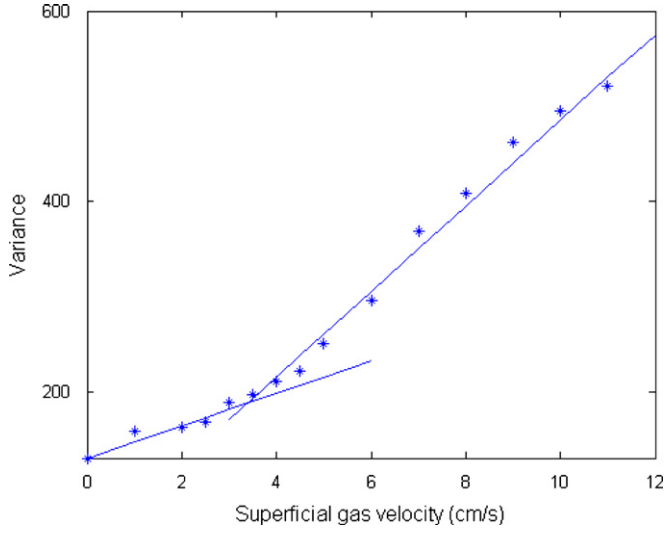

Fig. 8. Variation of the variance of photon counts fluctuations with superficial gas velocity in a 0.1012 m diameter column using air–water system at ambient conditions.

mean and the variance increase. In addition, the difference between the mean and the variance also appears to increase with an increase in superficial gas velocity. To account for such a deviation of the time-series from a Poisson distribution, a new coefficient was proposed, called the coefficient of departure from Poisson distribution, D_P, and defined as

$$D_P = \frac{(\text{Variance})_i}{(\text{Variance})_{\text{pd}}}, \tag{6}$$

where $(\text{variance})_i$ is the variance of the obtained photon counts history at a certain superficial gas velocity, and $(\text{variance})_{\text{pd}}$ is the variance of the obtained photon counts history at that velocity, if it had been a Poisson distribution, i.e., the mean.

This reduces Eq. (6) to

$$D_P = \frac{(\text{Variance})_i}{(\text{Mean})_i}. \tag{7}$$

Hence, it is the ratio of the variance and the mean of the obtained photon counts history at a certain superficial gas velocity.

The value of D_P in an empty scan and in water (no gas flow) was found to be, as expected, unity. With an increase in superficial gas velocity, the value of D_P departs from unity. Fig. 9 shows the change

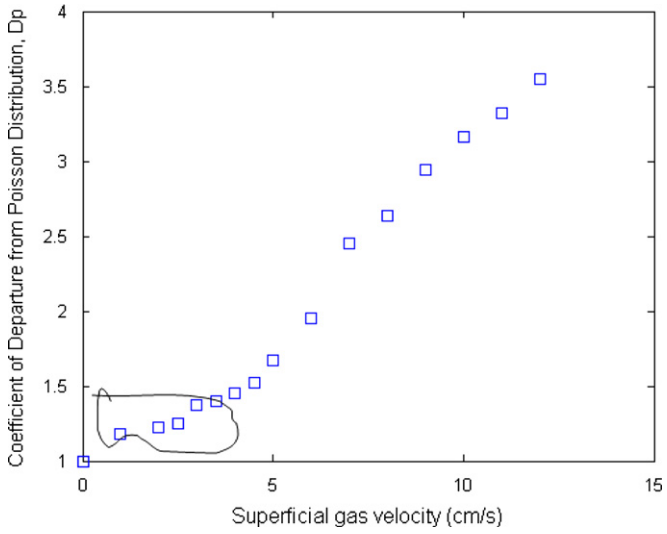

Fig. 9. The coefficient of departure from Poisson distribution versus superficial gas velocity in a 0.1012 m diameter column using an air–water system at ambient conditions.

in the coefficient of departure from a Poisson distribution with superficial gas velocity in a 0.1012 m diameter column using an air–water system. The value of D_P increases with an increase in superficial gas velocity. The rate of change in the value of D_P is less at low superficial gas velocities, but at higher superficial gas velocities it increases significantly with the change in superficial gas velocity. Only small bubbles are present in the system at low superficial gas velocities (in bubbly flow) that imparts fewer fluctuations around the mean, and hence the deviation with respect to the mean is less. However, in churn-turbulent flow, both small and large bubbles come in the path of γ-rays, which imparts intense fluctuations around the mean. Hence, the deviation of photon counts from the mean is significant at high superficial gas velocities.

It was observed that for superficial gas velocities above 3 cm/s, the value of D_P is greater than 1.4. Based on the conventional methods, the transition velocity was found to be around 3–4 cm/s; hence the behavior of the departure coefficient can be generalized based on the flow regime. It was found that in the churn-turbulent flow regime the value of D_P was greater than 1.4. It should be noted that, although the coefficient of departure from Poisson distribution has been defined based on the physics of γ-rays, its value for flow regime demarcation is purely empirical.

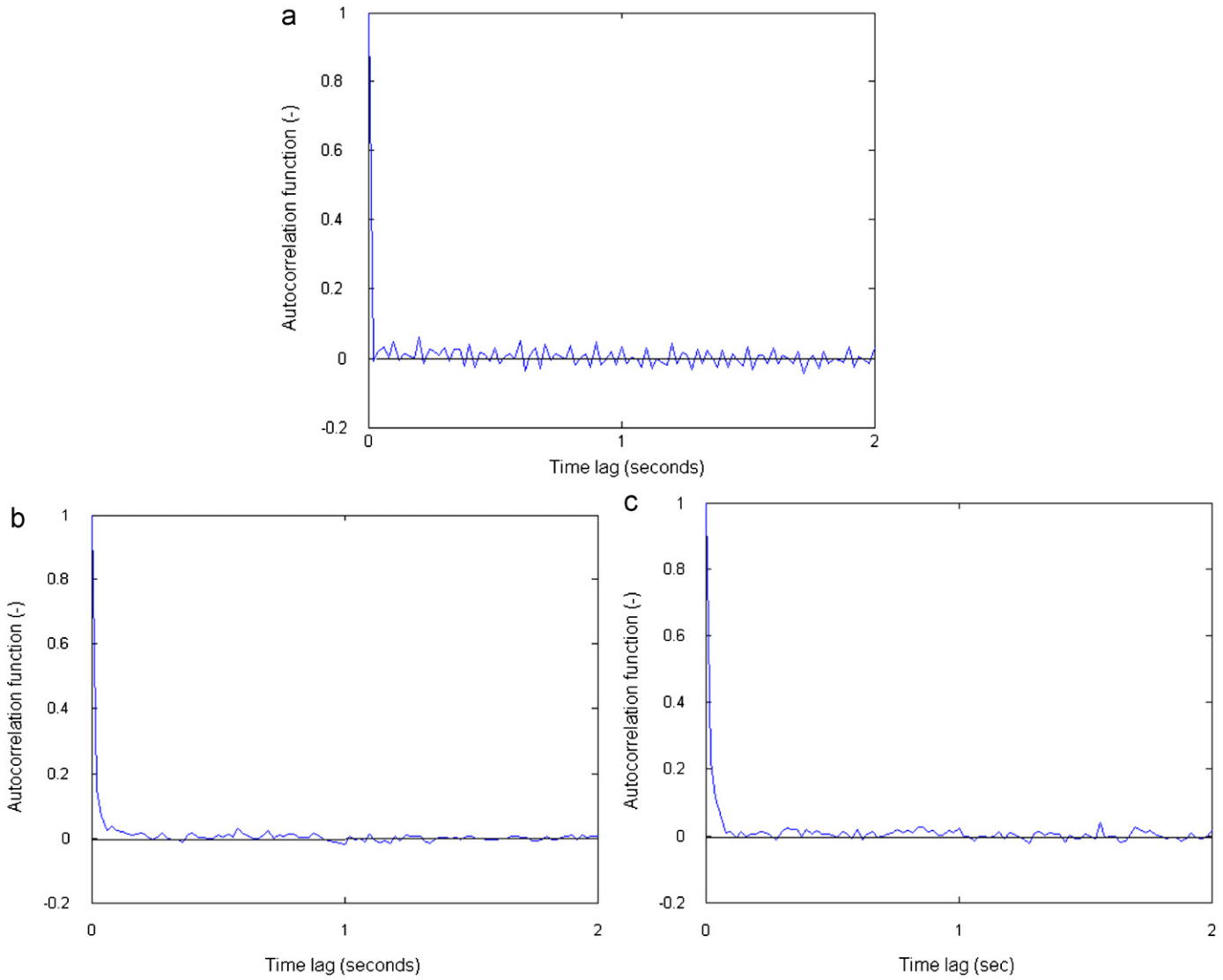

Fig. 10. Autocorrelation curve at superficial gas velocities of (a) 1, (b) 3, and (c) 4 cm/s using an air–water system in a 0.1012 m diameter column at ambient conditions.

The proposed coefficient facilitates identification of the underlying flow regime at the operating superficial gas velocity and promises to be a robust flow regime identifier in bubble columns.

3.2.3. Autocorrelation analysis

The autocorrelation function expresses the linear relationship between signal values at two different times and can be mathematically written as

$$C_{xx}(\tau) = \frac{1}{T}\int_{-\infty}^{+\infty} x(t)x(t-\tau).dt, \quad (8)$$

where τ is time lag, and μ and σ are the first and second moments of the distribution.

The autocorrelation function is used to estimate how well future values of a signal can be predicted from knowledge of the signal history. It provides information regarding the repetitiveness of a given signal. As long term processes do not appear in autocorrelation curves, they are generally evaluated over the time lag of 0–2 s without loss of any important information (Smith, 1999).

The obtained photon counts histories were subjected to autocorrelation analysis. Fig. 10 shows the autocorrelation curve, i.e., the autocorrelation coefficient versus time lag in bubbly flow at superficial gas velocities of (a) 1, (b) 3, and (c) 4 cm/s. The autocorrelation curves in bubbly flow exhibit the behavior of a typically random process and show a shape close to an exponential curve. In homogeneous flow, as the name suggests, due to the presence of uniform bubble sizes, the system is *virtually* similar everywhere. The events evolving over the time are similar in nature in bubbly flow. Hence, the time-series obtained in this regime is well correlated, as reflected in the autocorrelation curve.

Fig. 11 shows the autocorrelation curve in churn turbulent flows at superficial gas velocities of (a) 7, (b) 9, and (c) 11 cm/s. As the system enters into heterogeneous flow, the coalescence of small bubbles results in the appearance of larger bubbles, which in turn results into wider bubble size distribution. Hence, γ-rays encounter both small and large bubbles. Due to interception by bubbles of different sizes and characteristics, the probability of the same events evolving over time is relatively less, and hence the obtained series is not well correlated. This reflects in a characteristic anti-correlation superimposed on the exponential behavior in the autocorrelation curve in the churn-turbulent flow regime.

The autocorrelation curve shows close to exponential behavior in bubbly flows, while in churn-turbulent flows it exhibits characteristic anti-correlation behavior where cosine behavior is superimposed on an exponential curve. The visibly different behavior of the autocorrelation curves in the two regimes provides a means to demarcate them based on the shape of the autocorrelation curve at the operating condition.

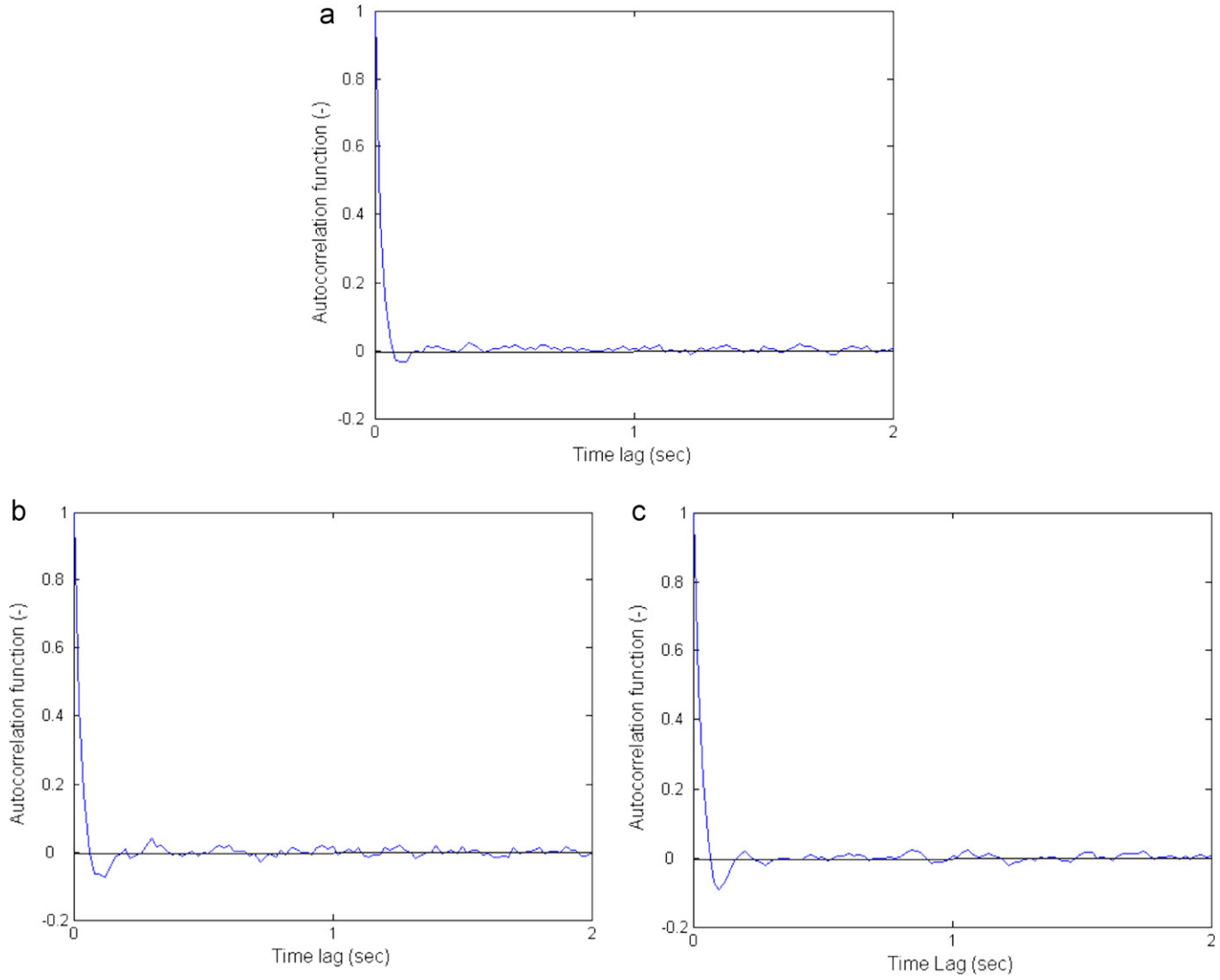

Fig. 11. Autocorrelation curve at superficial gas velocities of (a) 7, (b) 9, and (c) 11 cm/s using an air–water system in a 0.1012 m diameter column at ambient conditions.

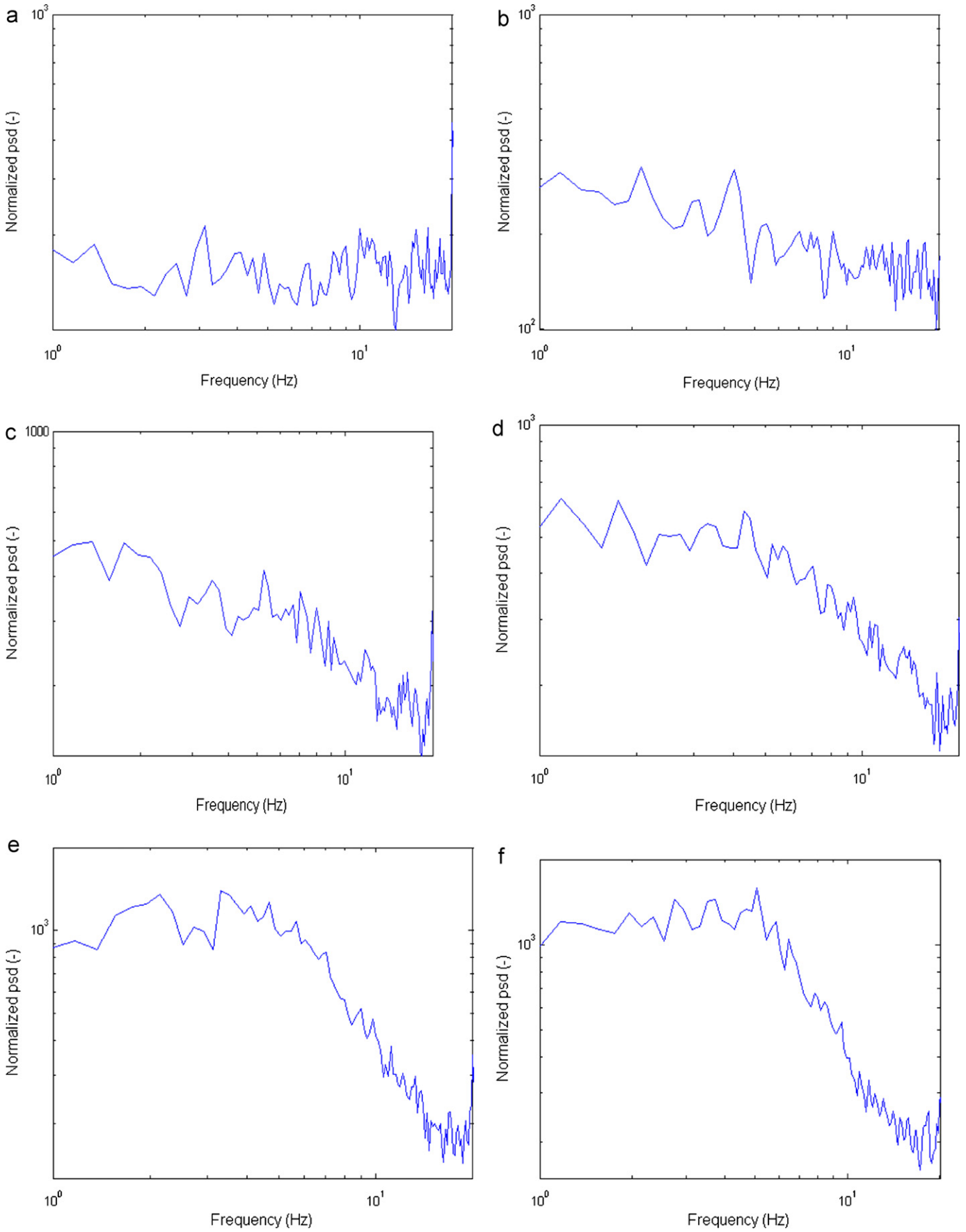

Fig. 12. Typical log–log plot of normalized psdf at superficial gas velocities of (a) 1, (b) 3, (c) 4, (d) 6, (e) 9, and (f) 11 cm/s, using an air–water system in a 0.1012 m diameter column at ambient conditions.

The behavior of the autocorrelation curves is a reflection of the nature of the time-series, irrespective of its operating and design conditions. Based on the inherent nature of the flow, the bubbly regime should exhibit correlated curve, while the churn-turbulent regime should exhibit an uncorrelated curve. This fact can be utilized for online flow regime identification in industrial reactors.

3.2.4. Spectral analysis

The goal of spectral analysis is to describe the distribution of the power contained in a signal over a frequency, based on a finite set of data. It converts information available in the time-domain into the frequency-domain.

Fourier transform, F, of a time series $x(t)$ can be given as

$$F(x) = \int_{-\infty}^{+\infty} x(t)\exp(-j2\pi f.t)dt, \quad (9)$$

where, f, is frequency.

The power spectral density (PSD),ϕ_{xx}, is the square of the magnitude of the continuous Fourier transform

$$\phi_{xx} = F(x).F*(x) \quad (10)$$

where $F^*(x)$ is the complex conjugate of Fourier transform.

Fig. 12 shows the log–log normalized psdf plots at superficial gas velocities of (a) 1, (b) 3, (c) 4, (d) 6, (e) 9, and (f) 11 cm/s. The normalized psdf is calculated by subtracting the original time-series from its mean. At 1 and 3 cm/s, i.e., in bubbly flow, the psdf plot did not show any power law fall off, while at higher superficial gas velocities, i.e., in the transition and churn-turbulent flow regimes, a distinct the power-law fall off was observed.

An analogy can be drawn between power-law fall off observed in the current study with that observed in single phase turbulent flow. In the bubble column literature, attempts have been made to apply the theory of isotropic turbulence. However, it should be noted here that the current study attempts neither to justify/evaluate the applicability of Kolmogorov's law for bubble columns nor to gain insights into such flows based on its applicability.

Zakrzewski et al. (1981) performed constant temperature film anemometer experiments to measure liquid velocity in a 0.14 m diameter and 2.69 m high column. The liquid phase was water and 1% Methanol. Two spargers were employed, viz., a sintered plate (pore diameter of 5 μm) and a perforated plate (home diameter=1 and 3 mm). They measured the turbulent intensities and determined the energy distribution spectra. Zakrzewski et al. (1981) found the slope of the log–log energy distribution plot to be −2 in the 'inertial subrange'. They concluded that Kolomogrov's law for single phase turbulence with −5/3 slope was derived for grid turbulence, whereas for the case of the bubble swarm turbulence in bubble columns, a slope of −2 is to be expected.

Lance and Bataille (1991) performed Laser Doppler Anemometry (LDA) and hot-film anemometry experiments in an air–water bubble column. The test section used in the study was a 2 m long square channel (0.45 × 0.45 m) operated at ambient conditions. The experimental conditions were such that the void fraction was varied between 0% and 3%. Lance and Bataille (1991) found that the classical −5/3 power law describing the behavior of the spectra in the high wavenumber range was progressively replaced by another power law of exponent equal to −8/3.

Recently, Groen (2004) performed LDA studies in an air–water system in three different column diameters, i.e., 15, 23, and 40 cm. Groen (2004) found the value of the slope to be in the range of −3/2 and −5/3. The close observation of psdf plots provided in Groen (2004) thesis shows that the frequency range where such a power law fall-off was observed depends on the radial location of the measurement. As one moves inwards to the column center, the power spectra also appear to shift inwards. The power-law fall-off seems to exist in the 'inertial subrange' for measurement locations close to the wall. However, such a slope was observed in far smaller frequency ranges for measurement locations towards the column center. The power spectra at a few measurement locations show a power-law fall off in the frequency range observed in the current work.

It is worth mentioning that in earlier studies, experiments were apparently performed in the bubbly flow regime. The power-law fall off was observed in homogeneous flow in these studies. In the current study, no such exponent was observed in bubbly flow. Based on this, further quantitative analysis was performed for observed power-law fall off in the psdf plot of photon counts history at higher superficial gas velocities in the current study.

The psdf plot of photon counts history obtained in an empty column (air) and water (with no gas flow) is shown in Fig. 13a and b. As mentioned earlier, a Poisson distribution was observed during scans in air and water (with no gas flow). The log–log normalized psdf plot does not show any variation in the power.

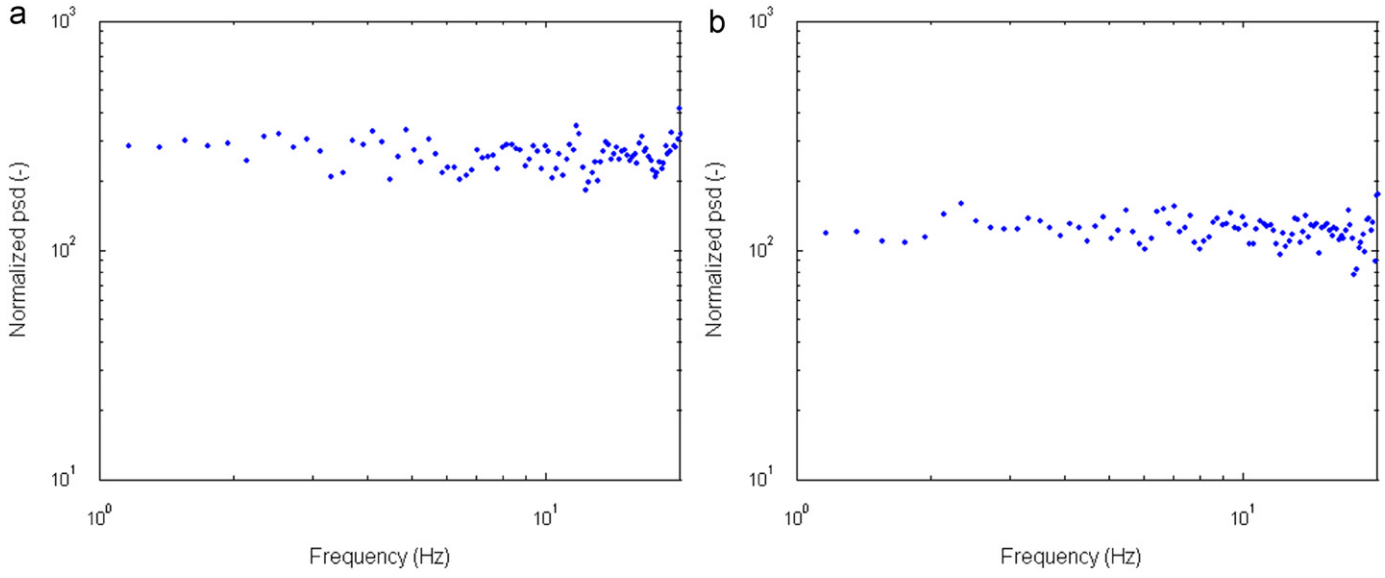

Fig. 13. Log–log plot of normalized psdf of photon counts history obtained in (a) empty column and (b) water (with no gas flow).

This is expected, as the photon counts obtained in air and water indicate characteristic noise inherent to gamma-rays. This rules out the possibility of occurrence of meaningful power spectra and its slope, due to the contribution of, or being an artifact of, a Poisson distribution.

Next, the operating conditions where the psdf plot showed a power-law fall off were analyzed. In general, the power-law fall off was observed in the frequency range of 5–15 Hz, and the data points in this range were regressed to obtain the best fit. The fitted equations are shown in Fig. 14a–d along with the R-squared value. The R-squared values were found to be equal to or greater than 0.85 in all the cases. At high superficial gas velocities, the R-squared values were close to 0.96.

The distinct slope in the psdf plot started to appear at a superficial gas velocity of 4 cm/s where the transition regime exists (Fig. 14a). The slope increases with an increase in superficial gas velocity. At a superficial gas velocity of 6 cm/s, the slope is close to −1 (Fig. 14b). Above superficial gas velocities of 6 cm/s, the slope gradually increases and remains close to −1.7 in fully churn-turbulent flow. Fig. 14c and d show the log–log plot of the normalized psdf at superficial gas velocities of 9 and 11 cm/s with an exponent close to −1.7. Table 2 shows the slopes of the power spectra at studied operating conditions. It is clear that Kolomogorov's −5/3 law appears to be applicable in the two phase churn-turbulent flow, as in a single phase turbulent flow, indicating that the mechanism of energy dissipation in two-phase flow is similar to that observed in single phase turbulent flows. However the power-law fall off was observed at relatively low frequencies during these studies.

In the current study, the exponent was observed in either transition or churn-turbulent flow regimes. The close observation of power spectra obtained in this study shows that the values of the power in water (with no gas flow) and the values in bubbly flows are close to each other, indicating that a Poisson distribution might be still dominant at these conditions. The value of the coefficient of a Poisson distribution also varies up to 1.2–1.3. At high superficial gas velocities the appearance of large bubbles increases the fluctuations in the system, adding significant flow dynamics information to a Poisson distribution. This might be a possible reason for the absence of the slope in power spectra in bubbly flow using NGD.

Apart from its analogy to a single phase turbulent flow, the observed slope can be utilized for the main objective of this study, i.e., to demarcate the underlying flow regime. It is worth mentioning that although the literature studies exhibit power law fall off in bubbly flow, such behavior was not observed in the current study. The current study observed power law fall-off in transition flow (-0.7), which gradually increased to −1.7 in churn-turbulent flow. The previous studies were performed using either LDA or a hot film anemometer. No experiments were performed during those studies in churn-turbulent flow.

Based on the available information and the current study, it can be concluded that no power law fall off in bubbly flow and power law fall off in the churn-turbulent flow can be exclusive characteristics of photon counts time-series obtained using NGD. The main goal of this study was not to analyze the power spectra or its utility in understanding the flow in bubble column. However, such an observation is helpful in developing a 'flow regime identifier' for NGD, which is the main objective of the current study.

4. Remarks

The current work demonstrated the ability of NGD to identify fingerprints of the prevailing hydrodynamic flow regime in bubble column reactors. Based on the studies performed in air–water system in 0.1012 m column and comparison with traditional flow regime identification methods, following 'flow regime identifiers' were developed for NGD,

(1) The newly proposed coefficient of departure of photon counts history is greater than 1.4 in the churn-turbulent flow.
(2) The autocorrelation curve exhibits different behaviors in bubbly and churn-turbulent flows. In bubbly flow, it exhibits a near exponential curve, while churn-turbulent flow exhibits anti-correlation behavior superimposed on an exponential curve.
(3) The normalized logarithmic psdf plot shows no slope in bubbly flow, while a distinct slope was observed in churn-turbulent flow.

The development of NGD, along with its identifiers, presents an opportunity to identify the prevailing flow regime without disturbing the process operation. As mentioned earlier, NGD can be mounted externally, and analyzing the obtained time-series at process conditions in the context of the developed identifiers can provide information regarding the prevailing flow regime. The developed method negates the need to observe the evolution of a secondary parameter over the range of superficial gas velocities for flow regime identification, and hence it can be applied without changing the process conditions.

Nomenclature

C_{xx}	Autocorrelation function, dimensionless
C_{xy}	Correlation function, dimensionless
D	Column diameter, m
f	Frequency, Hz
$F(x)$	Fourier transform of x
g	Gravity constant, m s^{-2}
j	Drift flux, m s^{-1}
L	Column length, m
N	Length of time series, dimensionless
n	Slope of gas holdup curve (Eq. 1), dimensionless
T	Length of time series, min
U_G	Superficial gas velocity, m s^{-1}
U_L	Superficial liquid velocity, m s^{-1}

Greek Letters

ε_G	Overall gas hold up, dimensionless
μ	Mean of a time-series, dimension of time-series
σ	Standard deviation of a time series, dimension of time-series
τ_0	Characteristic time-scale, s
ϕxy	Cross-spectral density function
τ	Time lag, s

Abbrevations

ACF	Autocorrelation function
CARPT	Computer automated radioactive particle tracking
CCF	Cross-correlation function
CT	Computed tomography
ECT	Electrical capacitance tomography
ERT	Electrical resistance tomography
LDA	Laser Doppler anemometry
NGD	Nuclear gauge densitometry
PDF	Probability density function
PIV	Particle image velocimetry
PSDF	Power spectral density function

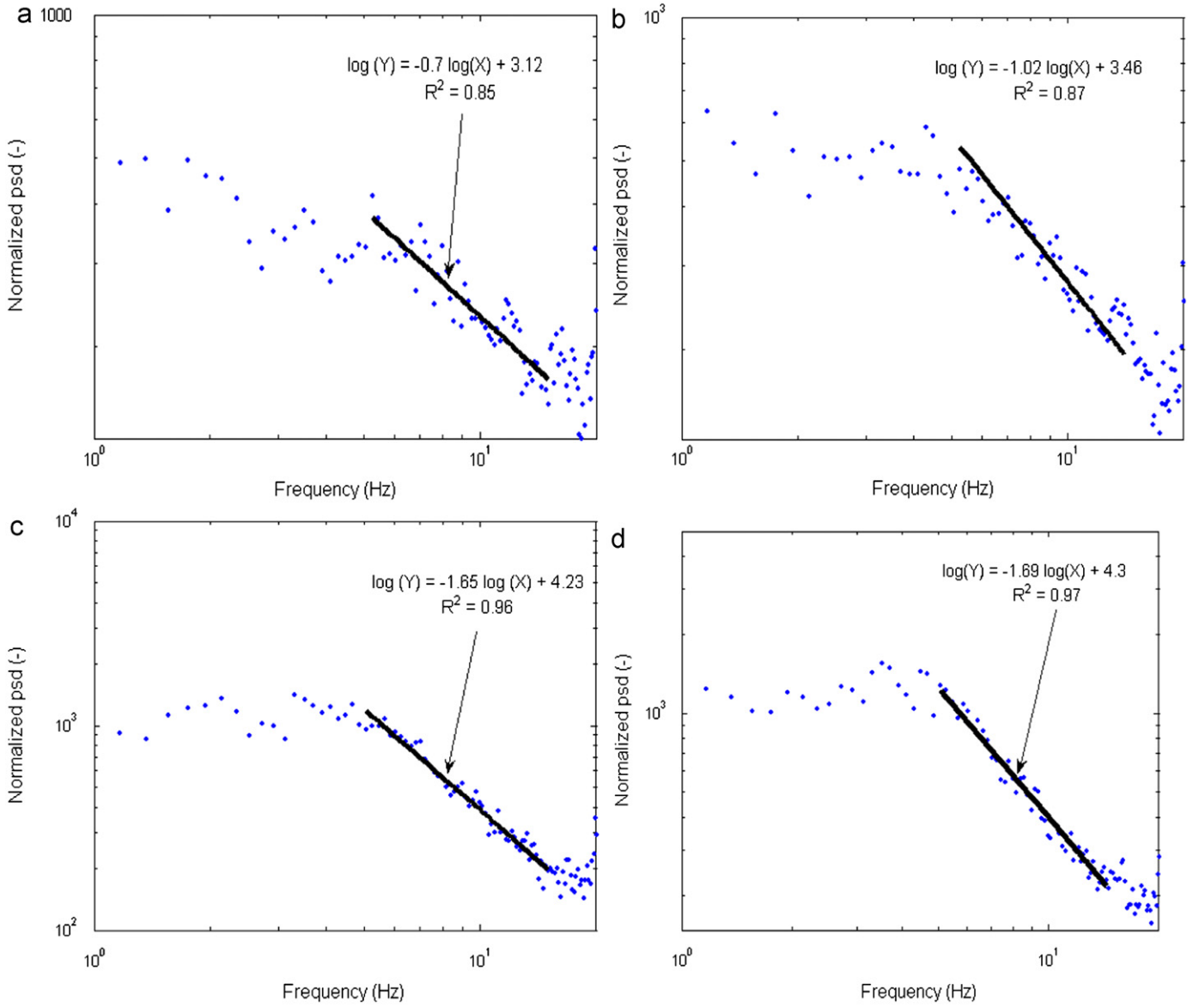

Fig. 14. Log–log plot of normalized psdf with fitted slope line at superficial gas velocities of (a) 4, (b) 6, (c) 9, and (d) 11 cm/s using an air–water system in a 0.1012 m diameter column at ambient conditions.

Table 2
Slope of power spectra at studied operating conditions.

Superficial gas velocity (cm/s)	Slope of power spectra
1	–
2	–
3	–
4	−0.7
5	−0.7
6	−1.02
7	−1.6
8	−1.62
9	−1.65
10	−1.67
11	−1.69
12	−1.7

Acknowledgments

The authors are thankful to the High Pressure Slurry Bubble Column Reactor (HPSBCR) Consortium [ConocoPhillips (USA), EniTech (Italy), Sasol (South Africa), Statoil (Norway)] and UCR-DOE (DE-FG-26-99FT40594) grants that made this work possible.

References

Al-Masry, W.A., Ali, E.M., Aqeel, Y.M., 2005. Determination of bubble characteristics in bubble columns using statistical analysis of acoustic sound measurements. Chem. Eng. Res. Des. 83 (A10), 1196–1207.

Bakshi, B.R., Zhong, H., Jiang, P., Fan, L.S., 1995. Analysis of flow in gas-liquid bubble columns using multi-resolution methods. Chem. Eng. Res. Des. 73 (A6), 608–614.

Bennett, M.A., West, R.M., Luke, S.P., Jia, X., Williams, R.A., 1999. Measurement and analysis of flows in gas-liquid column reactor. Chem. Eng. Sci. 54, 5003–5012.

Briens, L.A., Briens, C.L., Margaritis, A., Hay, J., 1997. Minimum liquid fluidization velocity in gas-liquid-solid fluidized bed of low-density particles. Chem. Eng. Sci. 52 (21–22), 4231–4238.

Carra, Sergio, Morbidelli, Massimo, 1987. Gas-liquid reactors. Chemical Industries (Dekker). Chem. React. React. Eng., 545–666.

Cassanello, M., Larachi, F., Kemoun, A., Al-Dahhan, M.H., Dudukovic, M.P., 2001. Inferring liquid chaotic dynamics in bubble columns. Chem. Eng. Sci. 56, 6125–6134.

Chen, R.C., Reese, J., Fan, L.-S., 1994. Flow structure in a three-dimensional bubble column and three-phase fluidized bed. AIChE J. 40 (7), 1093–1104.

Deckwer, W., 1992. Bubble Column Reactors. John Wiley & Sons.

Diesterwerg, G., Fuhr, H., Reher, P., 1978. Die Bayer-Turmbiologie. Industrieabwasser, 7.
Dong, Feng, Liu, Xiaoping, Deng, Xiang, Xu, Lijun, and Xu, Ling-au, (2001). Identification of two-phase flow regime using electrical resistance tomography, in: Proceedings of Second World Congress on Industrial Process Tomography, Hannover, Germany.
Drahos, J., Zahradnik, J., Puncochar, M., Fialova, M., Bradka, F., 1991. Effect of operating conditions on the characteristics of pressure fluctuations in a bubble column. Chem. Eng. Process. 29 (2), 107–115.
Fan, L.-S. (1989). Gas-Liquid-Solid Fluidization Engineering. Butterworth Series in Chemical Engineering, Boston, MA.
Groen, J. 2004. Scales and structures in bubbly flows. Ph.D. Thesis. Delft University of Technology. Delft, The Netherlands.
Holler, V., Ruzicka, M., Drahos, J., Kiwi-Minsker, L., Renken, A., 2003. Acoustic and visual study of bubble formation processes in bubble columns staged with fibrous catalytic layers. Catal. Today 79-80, 151–157.
Kikuchi, R., Yano, T., Tsutsumi, A., Yoshida, K., Punchochar, M., Drahos, J., 1997. Diagnosis of chaotic dynamics of bubble motion in a bubble column. Chem. Eng. Sci. 52 (21/22), 3741–3745.
Lance, M., Bataille, J., 1991. Turbulence in the liquid phase of a uniform bubbly air-water flow. J. Fluid Mech. 222, 95.
Lehman, J. and Hammer, J., (1978), Continuous fermentation in tower fermentor. I European Congress on Biotechnology, Interlaken, Part 1, 1.
Letzel, H.M., Schouten, J.C., Krishna, R., Van Den Bleek, C.M., 1997. Characterization of regimes and regime transitions in bubble columns by chaos analysis of pressure signals. Chem. Eng. Sci. 52 (24), 4447–4459.
Lin, T.-J., Reese, J., Hong, T., Fan, L.-S., 1996. Quantitative analysis and computation of two-dimensional bubble columns. AIChE J. 42 (2), 301–318.
Matsui, G., 1984. Identification of flow regimes in vertical gas-liquid two-phase flow using differential pressure fluctuations. Int. J. Multiphase Flow 10 (6), 711–720.
Murugaian, V., Schaberg, H.I., and Wang, M., (2005). Effect of sparger geometry on the mechanism of flow pattern transition in a bubble column. in: Proceedings of 4th World Congress on Industrial Process Tomography, Aizu, Japan.
Nedeltchev, Stoyan, Kumar, B., Dudukovic, M.P., 2003. Flow regime identification in a bubble column based on both Kolmogorov entropy and quality of mixedness derived from CARPT data. Can. J. Chem. Eng. 81, 367–374.
Nishikawa, K., Sekoguchi, K., Fukano, T., 1969. On the pulsation phenomena in gas-liquid two-phase flow. Bull. JSME 12 (54), 1410–1416.
Olmos, E., Gentric, C., Poncin, S., Midoux, N., 2003. Description of flow regime transitions in bubble columns via laser Doppler anemometry signals processing. Chem. Eng. Sci. 58 (9), 1731–1742.
Park, Soung Hee, Kim, Sang Done, 2003. Characterization of pressure signals in a bubble column by wavelet packet transform. Korean J. Chem. Eng. 20 (1), 128–132.
Rados, N. (2003). Slurry Bubble Column Hydrodynamics. D.Sc. Thesis, Washington University, St. Louis, MO.
Shaikh, Ashfaq, Al-Dahhan, Muthanna., 2005. Characterization of the hydrodynamic flow regime in bubble columns via computed tomography. Flow Meas. Instrum. 16 (2-3), 91–98.
Shaikh, Ashfaq, Al-Dahhan, Muthanna., 2007. A review on flow regime transition in bubble columns. Int. J. Chem. React. Eng. 5, R1.
Shaikh, A. (2007). Bubble and slurry bubble columns: mixing, flow regime transition, and scaleup. D.Sc. Thesis, Washington University, St. Louis, MO.
Smith, Steven, 1999. Digital Signal Processing. California Technical Publishing San Diego, California.
Thimmapuram, P.R., Rao, N.S., Saxena, S.C., 1992. Characterization of hydrodynamic regimes in a bubble column. Chem. Eng. Sci. 47 (13–14), 3335–3362.
Vial, C., Poncin, S., Wild, G., Midoux, N., 2001. A simple method for regime identification and flow characterisation in bubble columns and airlift reactors. Chem. Eng. Process. 40 (2), 135–151.
Wallis, G.B., 1969. One Dimensional Two Phase Flow. McGraw Hill, New York.
Wender, I., 1996. Reactions of synthesis gas. Fuel Process. Technol. 48, 189.
Zakrzewski, W., Lippert, J., Lübbert, A., Schügerl, K., 1981. Charakterisierung von blasensäulen durch turbulenzmessungen. Chem. Ing. Tech. 53 (2), 135.
Zhang, J.-P., Grace, J.R., Epstein, N., Lim, K.S., 1997. Flow regime identification in gas-liquid flow and three-phase fluidized beds. Chem. Eng. Sci. 52 (21/22), 3979–3992.